Hindawi
Discrete Dynamics in Nature and Society
Volume 2022, Article ID 6604684, 17 pages
https://doi.org/10.1155/2022/6604684

Research Article

A New Hyperchaotic Two-Scroll System: Bifurcation Study, Multistability, Circuit Simulation, and FPGA Realization

Sundarapandian Vaidyanathan,[1] **Aceng Sambas**,[2,3] **Esteban Tlelo-Cuautle**,[4] **Ciro Fabian Bermudez-Marquez**,[4] **Khaled Benkouider**,[5] **and Samy Abdelwahab Safaan**[6,7]

[1]*Centre for Control Systems, Vel Tech University, 400 Feet Outer Ring Road, Chennai 600062, India*
[2]*Mechanical Engineering Department, Universitas Muhammadiyah Tasikmalaya, Tasikmalaya, Jawa Barat 46196, Indonesia*
[3]*Institute of Strategic Industrial Decision Modelling (ISIDM), Universiti Utara Malaysia, Sintok, Kedah 06010, Malaysia*
[4]*Electronics Department, The National Institute of Astrophysics,Optics and Electronics (INAOE), Tonantzintla, Puebla 72840, Mexico*
[5]*Non Destructive Testing Laboratory, Automatic Department, Jijel University, BP 98, Jijel 18000, Algeria*
[6]*Department of Natural and Applied Sciences, Community College of Buraydah, Qassim University, Buraydah 52571, Saudi Arabia*
[7]*Nile Higher Institute for Commercial Science and Computer Technology, Mansoura 35511, Egypt*

Correspondence should be addressed to Sundarapandian Vaidyanathan; sundarcontrol@gmail.com

Received 8 July 2022; Accepted 23 August 2022; Published 22 September 2022

Academic Editor: Abdellatif Ben Makhlouf

With the swift advancement of chaos theory, the modeling, chaotic oscillations, and engineering applications of chaotic and hyperchaotic systems are important topics in research. In this research paper, we elucidate our findings of a new four-dimensional two-scroll hyperchaotic system having only two quadratic nonlinearities and carry out a detailed bifurcation study of the proposed dynamical model. Also, an electronic circuit has been constructed for the new system using MultiSim (Version 14). The implementation of the new 4-D hyperchaotic system in a field-programmable gate array (FPGA) is performed herein by applying two numerical methods, *viz*. Forward Euler Method and Trapezoidal Method. The experimental results show a good match with the simulated hyperchaotic attractors. We also provide details of the hardware resources used for an FPGA Basys 3 Xilinx Artix-7 XC7A35T-ICPG236C.

1. Introduction

Due to the rapid advancement of chaos theory, chaotic and hyperchaotic systems are applicable in several engineering branches such as memristive circuits [1–4], chemical oscillators [5–7], information sensing systems [8–10], lasers [11, 12], and communication systems [13–16]. Xiu et al. [17] designed a 5-D hyperchaotic system with hardware circuit design developed from a memristive cellular neural network (CNN) and applied it to build a secure communication system. Nazir et al. [18] proposed a secure communication system for encryption based on a 4-D hyperchaotic system and genetic codes. Bian and Yu [19] showed the use of a 6-D hyperchaotic system to enhance the security of a communication system. Boumaraf and Merazka [20] demonstrated the use of a new 4-D hyperchaotic cryptosystem for encryption applications.

Modeling of two-scroll hyperchaotic systems has attracted good research in the literature [21–23]. This research work reports the findings of a new four-dimensional nonlinear dynamical system having two quadratic nonlinear terms and depicting a two-scroll hyperchaotic attractor. Since the maximal Lyapunov exponent (MLE) of the two-scroll system is $\tau_{\max} = 2.6174$, we deduce that the two-scroll system (1) has high complexity. By a rigorous mathematical analysis, it is shown that the proposed mathematical model

has a unique balance point at the origin. This is followed by an extensive bifurcation analysis of the new 4-D two-scroll system reported in this work. We study the changes in the qualitative behavior of the proposed 4-D two-scroll system with respect to changes in the values of the system parameters by means of a bifurcation analysis. Bifurcation analysis for systems exhibiting chaos or hyperchaos is useful to get illuminated on the various qualitative properties like oscillations, quasi-periodicity, chaoticity, and hyperchaoticity when the parameters take various values in specified intervals [24–26]. Our research study also shows that the new hyperchaotic system exhibits multistability, which is a special property of coexistence of attractors for a selected set of values for the parameters but differing sets of values for the initial data of the trajectories [27, 28].

Circuit implementations of chaotic and hyperchaotic systems are of great usability in practice due to direct applications in many engineering disciplines [3, 29, 30]. An electronic model of the proposed hyperchaotic two-scroll system has been envisioned using MultiSim. Embedded and nonembedded implementations of chaotic and hyperchaotic systems are of paramount importance to increase their applications in many scientific and engineering fields since those FPGA designs can be linked directly to the digital world [31–35]. FPGA implementation of the proposed hyperchaotic two-scroll system has also been carried out at the end of this work by applying two numerical methods, *viz.* Forward Euler Method and Trapezoidal Method. Experimental implementation using FPGA facilitates practical applications with the new hyperchaotic model.

2. A New Hyperchaotic System with Two-Scroll Attractor

A two-scroll attractor of a new hyperchaotic system is the main contribution of the modelling part of this research paper. Our new system is the following 4-D dynamics given by

$$\dot{z} = f(z), \text{where } f(z) = \begin{bmatrix} a(z_2 - z_1) - z_3 + z_4 \\ cz_1 - z_2 - z_1 z_3 + z_4 \\ -bz_3 + z_1 z_2 \\ -dz_2 \end{bmatrix}. \tag{1}$$

In the 4-D dynamics (1), $z = (z_1, z_2, z_3, z_4)$ and a, b, c, d are positive system constants. We note that the vector field $f(z)$ has nine linear terms and two quadratic nonlinear terms.

When we take the constants as $(a, b, c, d) = (25, 8, 90, 6)$ and the initial data as $z(0) = (0.8, 0.2, 0.4, 0.6)$, the Lyapunov characteristic exponents of the model (1) can be estimated using MATLAB for $T = 1E4$ seconds as follows:

$$\begin{cases} \tau_1 = 2.6174, \\ \tau_2 = 0.2743, \\ \tau_3 = 0, \\ \tau_4 = -36.8194. \end{cases} \tag{2}$$

We note that the sum of the Lyapunov characteristic exponents of the model (1) is a negative quantity, *viz.*

$$\tau_1 + \tau_2 + \tau_3 + \tau_4 = -33.9277. \tag{3}$$

This calculation demonstrates that the 4-D system stated in the equation (1) has a dissipative hyperchaotic attractor with two positive Lyapunov characteristic exponents.

If $V(t)$ denotes a volume element of the flow of the 4-D hyperchaotic system (1), then the divergence of the flow of V is calculated as follows:

$$\nabla \cdot V = \frac{\partial f_1}{\partial z_1} + \frac{\partial f_2}{\partial z_2} + \frac{\partial f_3}{\partial z_3} + \frac{\partial f_4}{\partial z_4} = -a - b - 1. \tag{4}$$

This also shows that 4-D hyperchaotic system (1) is dissipative for all positive values of the system constants a and b. Since the maximal Lyapunov exponent (MLE) of the two-scroll system is $\tau_{\max} = 2.6174$, we deduce that the two-scroll system (1) has high complexity.

Figure 1 shows various MATLAB signal portraits of the 4-D hyperchaotic two-scroll dynamics (1) for the initial data $z(0) = (0.8, 0.2, 0.4, 0.6)$ and parameter data $(a, b, c, d) = (25, 8, 90, 6)$.

The Kaplan–Yorke dimension of the 4-D hyperchaotic two-scroll dynamics (1) can be found as

$$D_{KY} = 3 + \frac{\tau_1 + \tau_2 + \tau_3}{|\tau_4|} = 3.0785. \tag{5}$$

The balance points (or equilibrium points) of system (1) are the roots of the system:

$$f(z) = 0. \tag{6}$$

Thus, we proceed to find the roots of the following nonlinear system:

$$a(z_2 - z_1) - z_3 + z_4 = 0, \tag{7a}$$

$$cz_1 - z_2 - z_1 z_3 + z_4 = 0, \tag{7b}$$

$$-bz_3 + z_1 z_2 = 0, \tag{7c}$$

$$-dz_2 = 0. \tag{7d}$$

Let us assume that $a > 0$, $b > 0$,$c > 0$, and $d > 0$.

From (7d), $-dz_2 = 0$ or $z_2 = 0$.

When we substitute $z_2 = 0$ in (7c), we get $-bz_3 = 0$ or $z_3 = 0$.

Furthermore, substitution of $z_2 = z_3 = 0$ into equations (7a) and (7b) lead to the following:

$$-az_1 + z_4 = 0, \tag{8a}$$

$$cz_1 + z_4 = 0. \tag{8b}$$

Subtracting (8a) from (8b), we get

$$(c + a)z_1 = 0. \tag{9}$$

Since c and a are positive constants, $c + a > 0$.

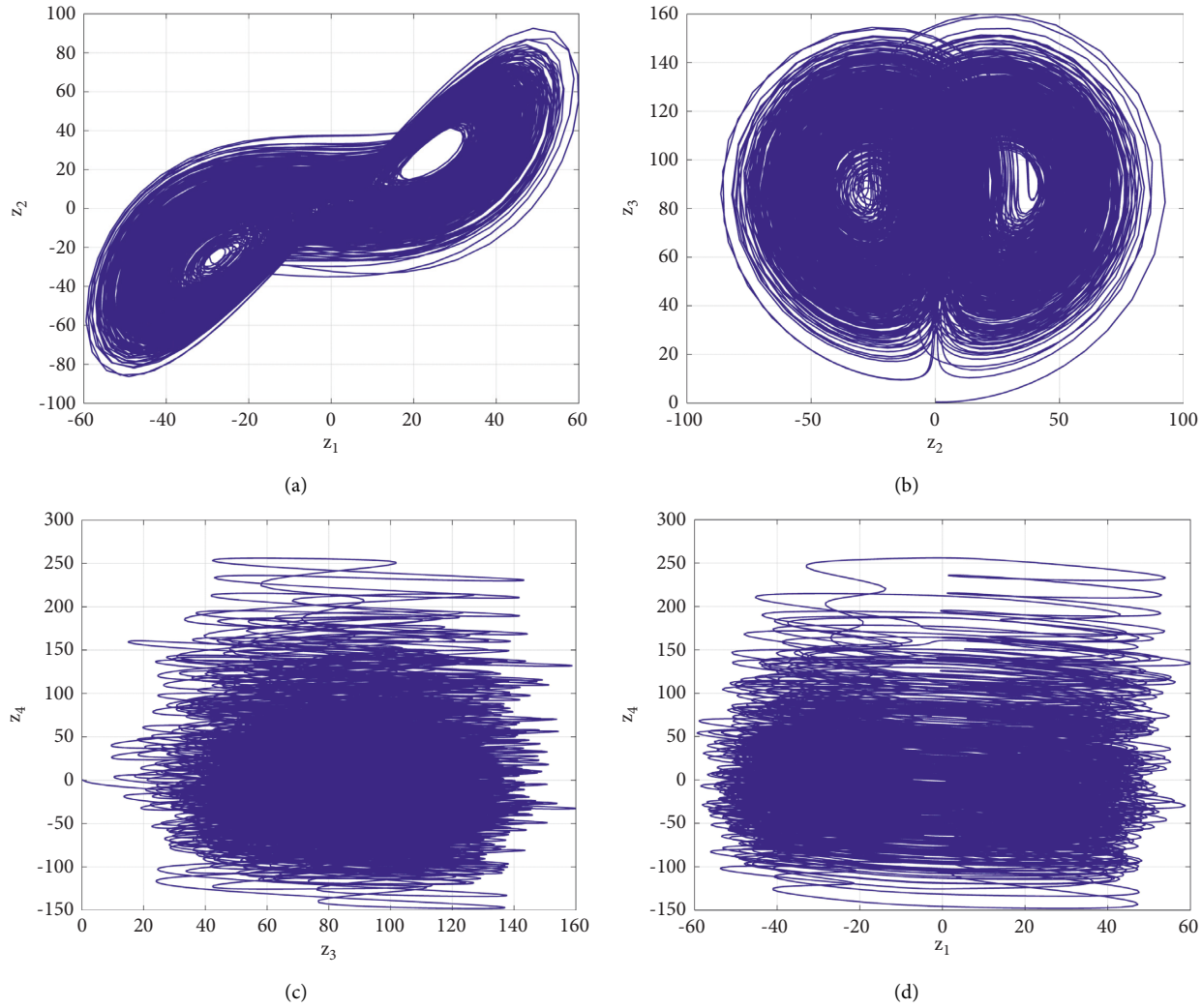

Figure 1: Various MATLAB signal portraits of the 4-D hyperchaotic two-scroll dynamics (1).

From (9), we get $z_1 = 0$.

Substituting $z_1 = 0$ into (8a) or (8b), we get $z_4 = 0$.

As a result of this calculation, we conclude that $Z_0 = 0$ is the only balance point for the 4-D two-scroll hyperchaotic system (1). The stability nature of $Z_0 = 0$ is found by calculating the eigenvalues of the Jacobian matrix $A = Df(0)$.

We take the constants for the hyperchaos case as $(a, b, c, d) = (25, 8, 90, 6)$.

For these values, we calculate the system Jacobian matrix as

$$A = Df(0) = \begin{bmatrix} -25 & 25 & -1 & 1 \\ 90 & -1 & 0 & 1 \\ 0 & 0 & -8 & 0 \\ 0 & -6 & 0 & 0 \end{bmatrix}. \tag{10}$$

With the use of MATLAB, we estimate the eigenvalues of the matrix A as

$$\begin{cases} \lambda_1 = 0.3121, \\ \lambda_2 = 35.6688, \\ \lambda_3 = -8.0000, \\ \lambda_4 = -61.9809. \end{cases} \tag{11}$$

This pinpoints that the unique balance point $Z_0 = 0$ of the two-scroll system (1) is a saddle-point, which is unstable. Hence, the model (1) has a self-excited two-scroll hyperchaotic attractor.

3. A Bifurcation Study of the Hyperchaotic Two-Scroll Attractor

In this section of the paper, the dynamical behavior of the novel, extremely complex two-scroll hyperchaotic system (1) is examined with $Z(0) = (0.8, 0.2, 0.4, 0.6)$.

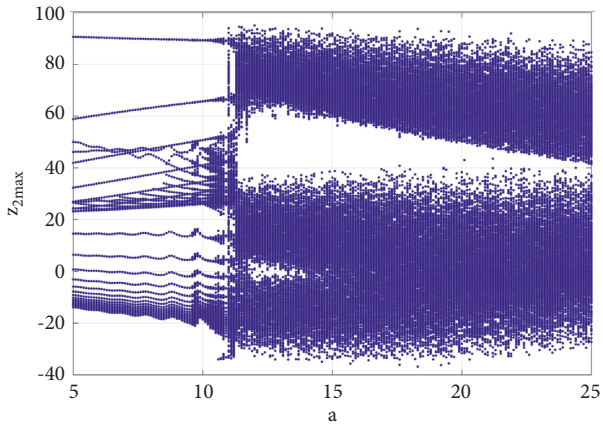

Figure 2: Bifurcation diagram for the model (1) when a varies in $[5, 25]$ and $(b, c, d) = (8, 90, 6)$.

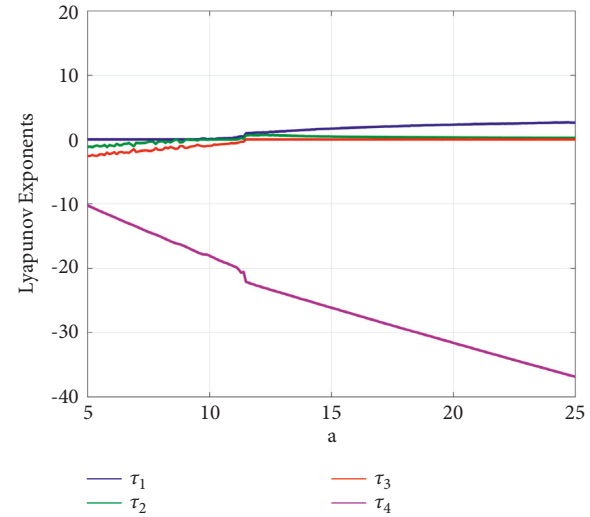

Figure 3: Lyapunov exponents for the model (1) when a varies in $[5, 25]$ and $(b, c, d) = (8, 90, 6)$.

3.1. Behavior Evolution When a Changes. Here, with the values of the constants b, c, d set to $b = 8$, $c = 90$ and $d = 6$, the dynamic responses of the 4-D dynamical system (1) are displayed when the value of the constant a increases in the interval of values [5, 25]. The outcomes of the simulation show that, depending on the value of parameter a, system (1) can display a variety of types of behavior such as periodic, chaotic, or hyperchaotic behavior with varying degrees of complexity. Figure 2 displays the bifurcation diagram for system (1). Figure 3 depicts the Lyapunov exponents (LE) spectrum $(\tau_1, \tau_2, \tau_3, \tau_4)$ for system (1).

From Figures 2 and 3, it can be seen that there are no positive LE value for system (1) in the range of $5 < a < 9.5$. Figure 4 shows a periodic response for system (1) when $a = 6$. The corresponding LE values of (1) are estimated using MATLAB as follows:

$$\tau_1 = 0, \tau_2 = -0.959, \tau_3 = -2.141, \tau_4 = -11.901. \quad (12)$$

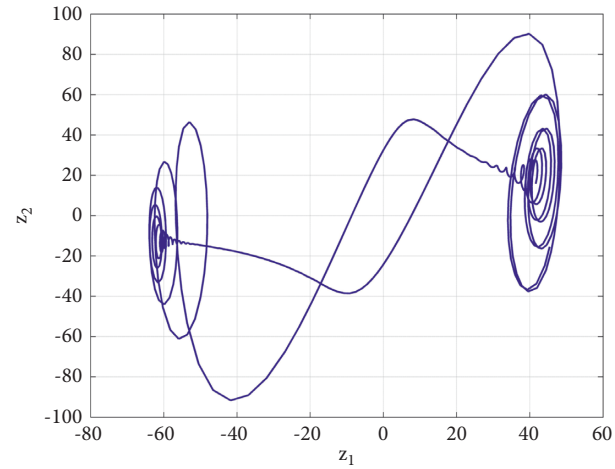

Figure 4: A periodic response of the model (1) for $a = 6$ and $(b, c, d) = (8, 90, 6)$.

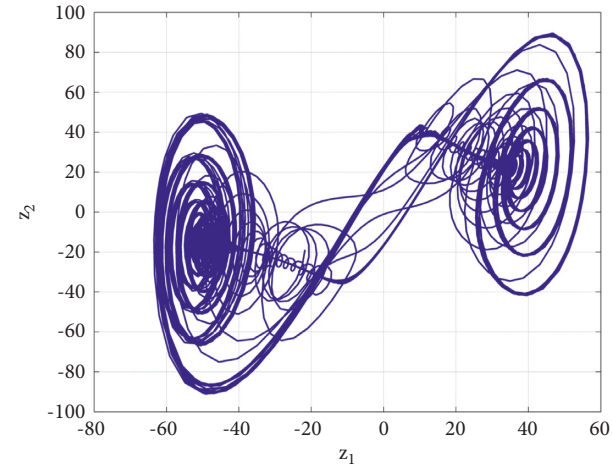

Figure 5: A chaotic attractor of the model (1) for $a = 11$ and $(b, c, d) = (8, 90, 6)$.

When $9.5 < a < 11.4$, τ_1 increases from zero to a positive value while τ_2 reaches zero. These results indicate that system (1) has a chaotic attractor for this range of parameter a, as clearly seen in Figure 5, when $a = 11$. The corresponding LE values of the new 4-D system are estimated using MATLAB as follows:

$$\tau_1 = 0.296, \tau_2 = 0, \tau_3 = -0.593, \tau_4 = -19.703. \quad (13)$$

Also, when $a = 11$, system (1) has a fractional Kaplan–York dimension:

$$D_{KY} = 2 + \frac{\tau_1 + \tau_2}{|\tau_3|} = 2.4992. \quad (14)$$

When $11.4 < a < 2.5$, system (1) has two positive LE values, which leads into a hyperchaotic region. Figure 6 presents the hyperchaotic attractor generated by system (1) when $a = 12$. The corresponding LE values of (1) are estimated using MATLAB as follows:

$$\tau_1 = 1.065, \tau_2 = 0.691, \tau_3 = 0, \tau_4 = -22.758. \quad (15)$$

Also, when $a = 12$, system (1) has a fractional Kaplan–York dimension:

$$D_{KY} = 3 + \frac{\tau_1 + \tau_2 + \tau_3}{|\tau_4|} = 3.0772. \quad (16)$$

From Figure 3, it can be seen that τ_1 increases with the increase of parameter a, until it reaches over 2.6 when $a = 25$. This causes more disordering in the attractor, as shown in Figure 7. Figures 4–7 portray a 2-D plot of the attractor of the 4-D system (1) in (z_1, z_2) coordinate plane for different values of the system constant a, while $(b, c, d) = (8, 90, 6)$.

3.2. Behavior Evolution When b Changes. Here, with the values of the constants b, c, d set to $a = 25$, $c = 90$, and $d = 6$, the dynamic responses of the 4-D dynamical system (1) are displayed when the value of the constant b increases in the interval of values $[8, 20]$. The outcomes of the simulation show that, depending on the value of parameter b, system (1) can display a variety of types of behavior such as periodic, chaotic, or hyperchaotic behavior with varying degrees of complexity. Figure 8 displays the bifurcation diagram for system (1). Figure 9 depicts the LE spectrum $(\tau_1, \tau_2, \tau_3, \tau_4)$ for system (1).

From Figures 8 and 9, it can be seen that τ_1 decreases with the increase of the constant b. When $8 < b < 14$, system (1) possesses two positive LE values. Figure 10 shows the hyperchaotic attractor of system (1) when $b = 10$. The corresponding LE values of (1) are estimated using MATLAB as follows:

$$\tau_1 = 2.666, \tau_2 = 0.273, \tau_3 = 0, \tau_4 = -38.942. \quad (17)$$

Also, when $b = 10$, system (1) has a fractional Kaplan–York dimension:

$$D_{KY} = 3 + \frac{\tau_1 + \tau_2 + \tau_3}{|\tau_4|} = 3.0755. \quad (18)$$

When $b = 13.8$, system (1) exhibits a less disordered hyperchaotic attractor shown in Figure 11, when compared with the one in Figure 10. The hyperchaotic attractor exhibited in Figure 11 has $\tau_1 = 2.442$ and $D_{KY} = 3.064$.

When $14 < b < 15$ the second Lyapunov exponent τ_2 decreases from a positive value to zero while the first exponent τ_1 stays still positive. This transition indicates that system (1) has a chaotic response for this range of parameter b. Figure 12 shows the chaotic attractor of system (1) when $b = 15$. This strange attractor is characterized by the following Lyapunov exponents:

$$\tau_1 = 0.061, \tau_2 = 0, \tau_3 = -0.772, \tau_4 = -40.284. \quad (19)$$

Also, when $b = 10$, system (1) has a fractional Kaplan–York dimension:

$$D_{KY} = 2 + \frac{\tau_1 + \tau_2}{|\tau_3|} = 2.0790. \quad (20)$$

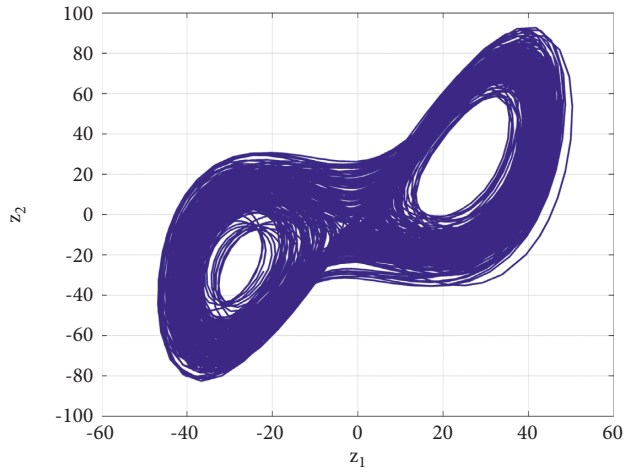

Figure 6: A hyperchaotic attractor of model (1) for $a = 12$ and $(b, c, d) = (8, 90, 6)$.

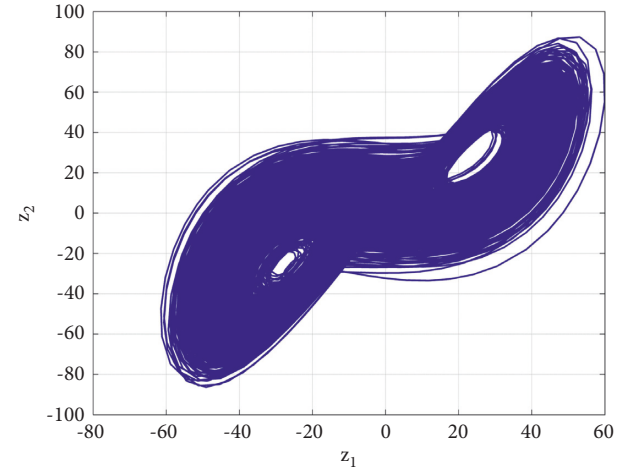

Figure 7: A hyperchaotic attractor of the model (1) when $a = 25$ and $(b, c, d) = (8, 90, 6)$.

When $15 < b < 20$, there are no positive exponents which mean that system (1) has a periodic response in this region of parameters. The periodic orbit is shown in Figure 13 when $b = 20$. The corresponding Lyapunov exponents are calculated and obtained as follows:

$$\tau_1 = 0, \tau_2 = -1.794, \tau_3 = -2.083, \tau_4 = -42.124. \quad (21)$$

Figures 10–12 and 1 portray a 2-D plot of the attractor of the 4-D system (1) in (z_1, z_3) coordinate plane for different values of the system constant b, while $(a, c, d) = (25, 90, 6)$.

3.3. Behavior Evolution When c Changes. Here, with the values of the constants a, b, d set to $a = 25$, $b = 8$, and $d = 6$, the dynamic responses of system (1) are displayed when the value of the constant c increases in the interval of values $[30, 90]$. The outcomes of the simulation show that, depending on the value of parameter c, system (1) can display a variety of types of behavior such as periodic, chaotic, or hyperchaotic behavior with varying degrees of

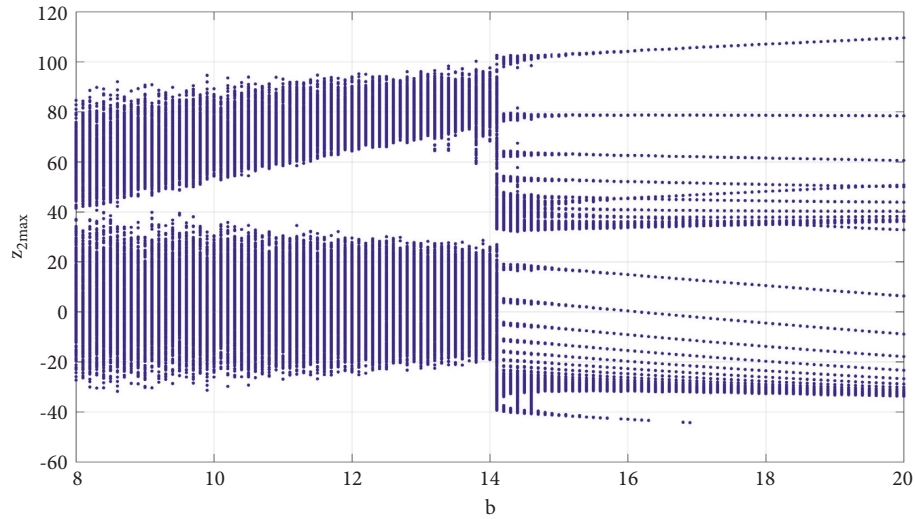

FIGURE 8: Bifurcation diagram for the model (1) when b varies in $[8, 20]$ and $(a, c, d) = (25, 90, 6)$.

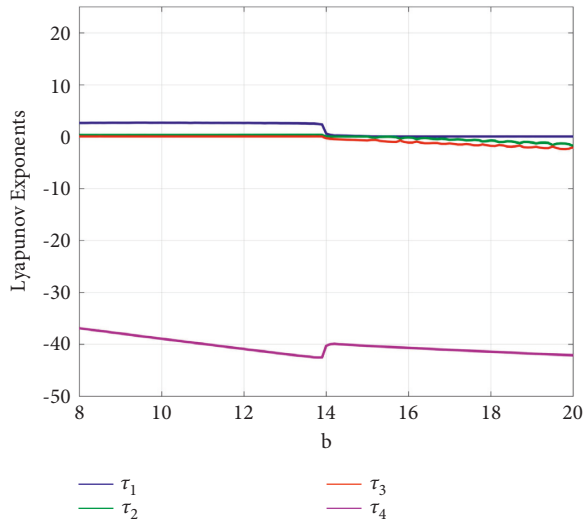

FIGURE 9: Lyapunov exponents for the model (1) when b varies in $[8, 20]$ and $(a, c, d) = (25, 90, 6)$.

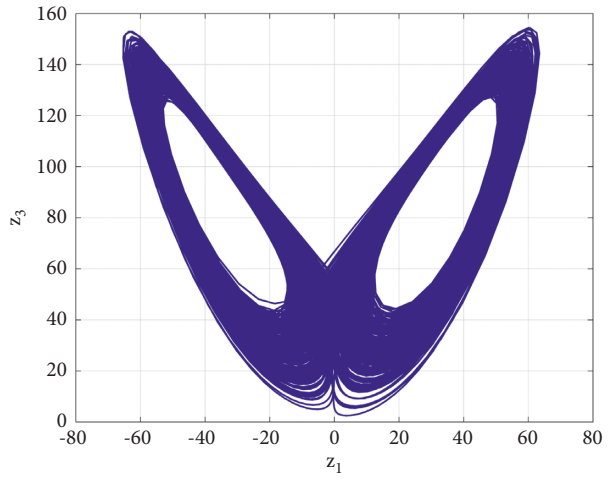

FIGURE 11: A hyperchaotic attractor of the model (1) for $b = 13.8$ and $(a, c, d) = (25, 90, 6)$.

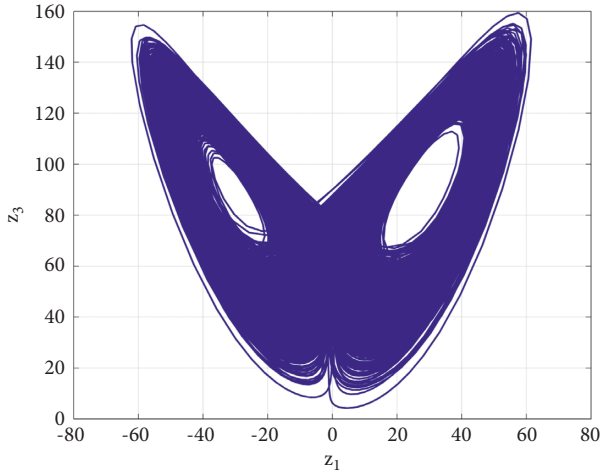

FIGURE 10: A hyperchaotic attractor of the model (1) for $b = 10$ and $(a, c, d) = (25, 90, 6)$.

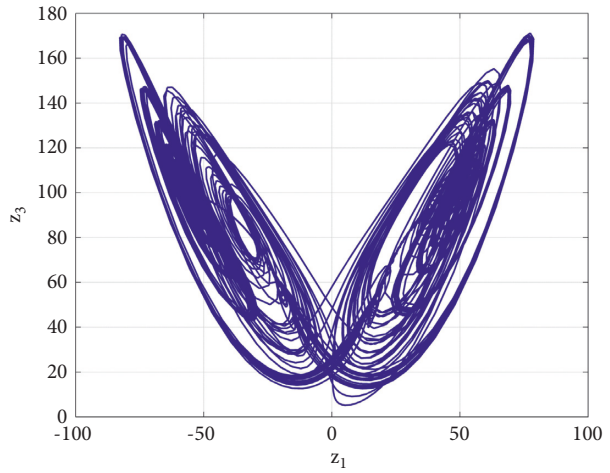

FIGURE 12: A chaotic attractor of the model (1) for $b = 15$ and $(a, c, d) = (25, 90, 6)$.

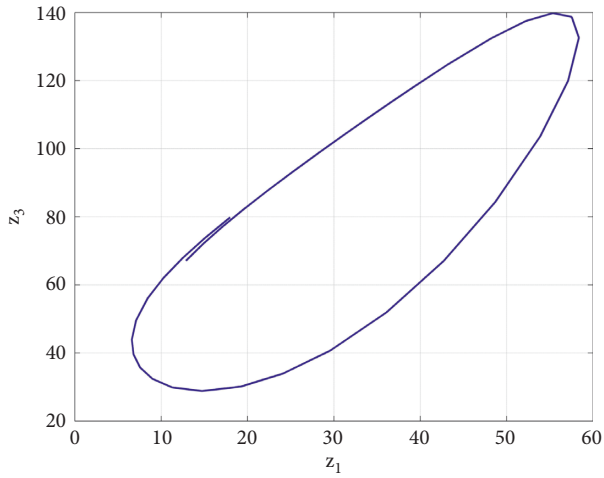

Figure 13: A periodic attractor of the model (1) for $b = 20$ and $(a, c, d) = (25, 90, 6)$.

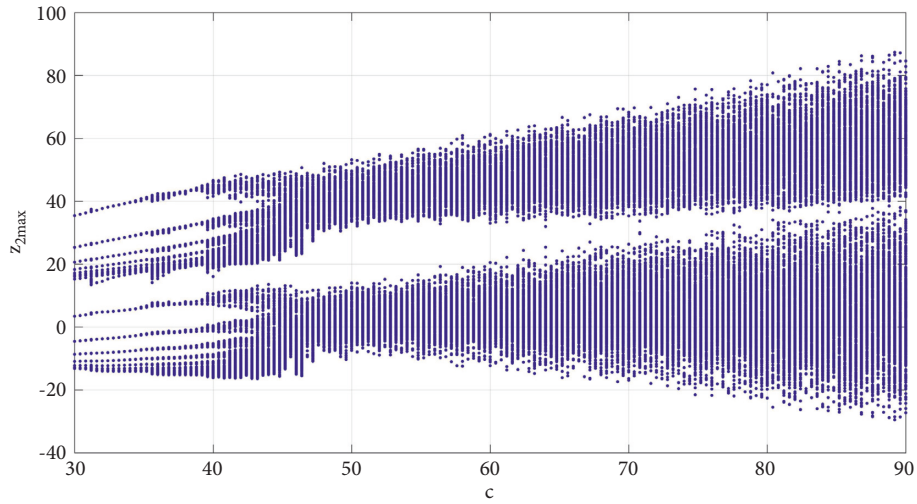

Figure 14: Bifurcation diagram for the model (1) when c varies in $[30, 90]$ and $(a, b, d) = (25, 8, 6)$.

complexity. Figure 14 displays the bifurcation diagram for system (1). Figure 15 depicts the LE spectrum $(\tau_1, \tau_2, \tau_3, \tau_4)$ for system (1).

From Figures 14 and 15, it can be seen that the first Lyapunov exponent τ_1 increases with the increase of the constant c. We define $A = [30, 30.9] \cup [31.5, 35.1] \cup [37.5, 39]$. When $c \in A$, system (1) does not have any positive LE value. Hence, system (1) has a periodic attractor for the values of c in this region. Figure 16 shows the periodic attractor of system (1) when $c = 30.5$. The corresponding LE values of (1) are estimated using MATLAB as follows:

$$\tau_1 = 0, \tau_2 = -0.222, \tau_3 = -1.035, \tau_4 = -32.744. \quad (22)$$

We define $B = [30.9, 31.5] \cup [35.1, 37.5] \cup [39, 44.7]$. When $c \in B$,τ_1 increases from zero to a positive value while the second Lyapunov exponent τ_2 reaches zero. These results indicate that system (1) has a chaotic behavior for this range of the constant $c \in B$. Figure 17 shows the chaotic attractor

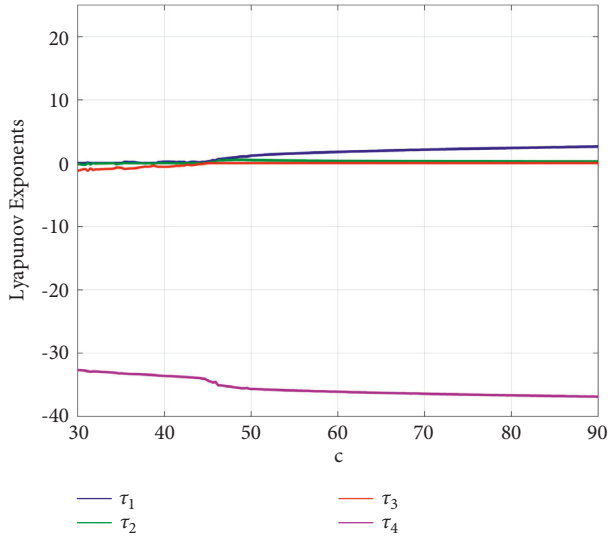

Figure 15: Lyapunov exponents for the model (1) when c varies in $[30, 90]$ and $(a, b, d) = (25, 8, 6)$.

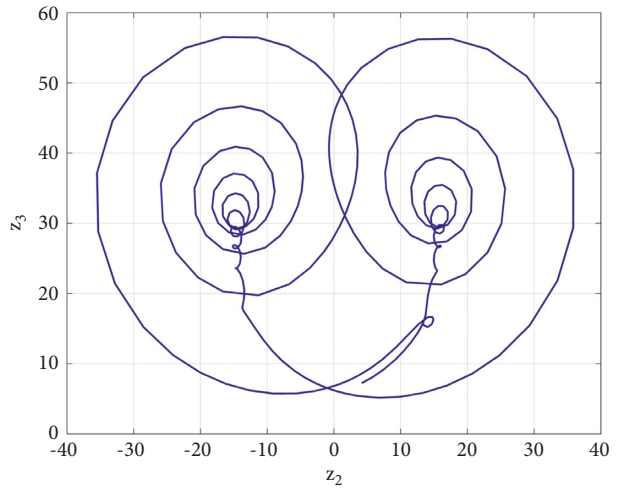

Figure 16: A periodic attractor of the 4-D system (1) when $c = 30.5$ and $(a, b, d) = (25, 8, 6)$.

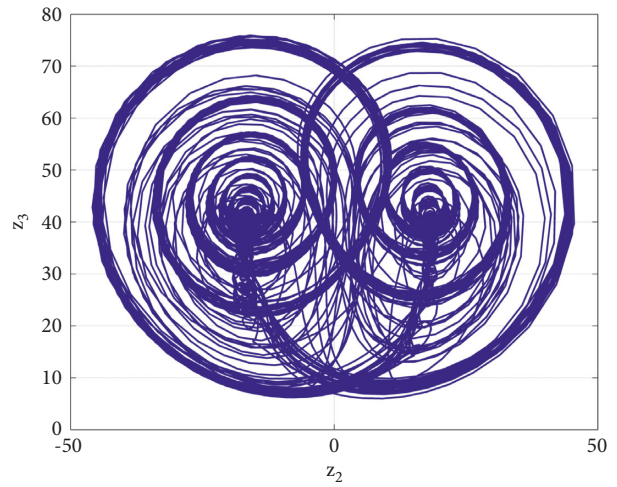

Figure 17: A chaotic attractor of the 4-D system (1) when $c = 40$ and $(a, b, d) = (25, 8, 6)$.

of system (1) when $c = 40$. The corresponding LE values of (1) are estimated using MATLAB as follows:

$$\tau_1 = 0.218, \tau_2 = 0, \tau_3 = -0.601, \tau_4 = -33.618. \quad (23)$$

Also, the Kaplan–Yorke dimension of (1) for $c = 40$ is obtained as:

$$D_{KY} = 2 + \frac{\tau_1 + \tau_2}{|\tau_3|} = 2.3627. \quad (24)$$

When $44.7 < c < 90$, system (1) has two positive LE values, which leads into a wide hyperchaotic region. Figure 18 presents the hyperchaotic attractor exhibited by (1) when $c = 50$.

The corresponding LE values of (1) are estimated using MATLAB as follows:

$$\tau_1 = 1.130, \tau_2 = 0.497, \tau_3 = 0, \tau_4 = -35.629. \quad (25)$$

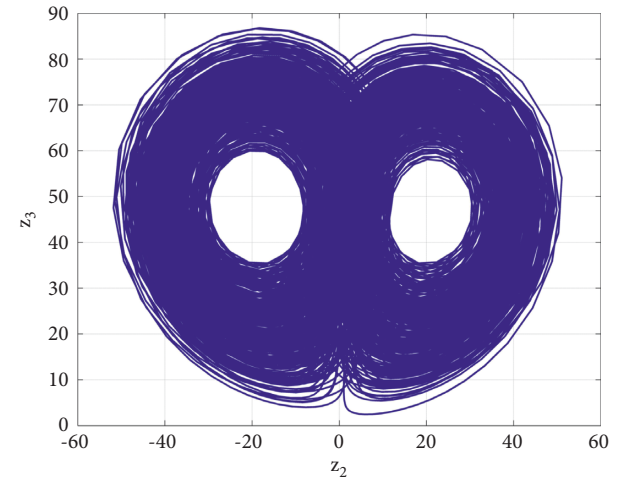

Figure 18: A hyperchaotic attractor of the model (1) for $c = 50$ and $(a, b, d) = (25, 8, 6)$.

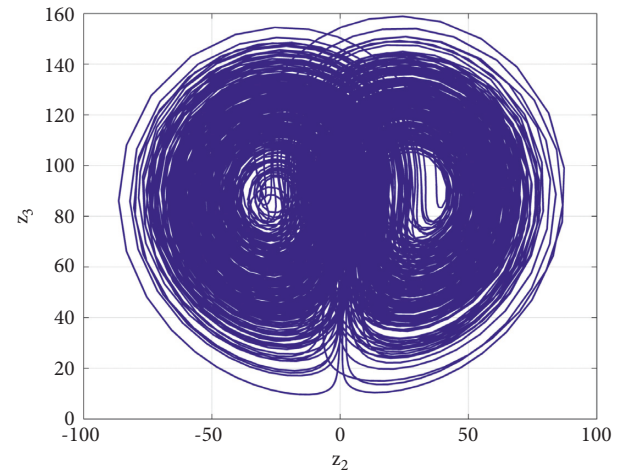

Figure 19: A hyperchaotic attractor of the model (1) for $c = 90$ and $(a, b, d) = (25, 8, 6)$.

Also, the Kaplan–Yorke dimension of (1) for $c = 50$ is obtained as:

$$D_{KY} = 3 + \frac{\tau_1 + \tau_2 + \tau_3}{|\tau_4|} = 3.0457. \quad (26)$$

From Figure 15, it can be seen that τ_1 increases with the increase of the constant c until it reaches over $\tau_1 = 2.6$ when $c = 90$. This causes a hyperchaotic attractor in which the trajectory is highly disordered, as seen in Figure 19.

Figures 16–19 portray a 2-D plot of the attractor of system (1) in (z_2, z_3) coordinate plane for different values of the constant c, while $(a, b, d) = (25, 8, 6)$.

3.4. Behavior Evolution When d Changes. Here, with the values of the constants a, b, c set to $a = 25$, $b = 8$, and $c = 90$, the dynamic responses of system (1) are displayed when the value of the constant d increases in the range of values $[5, 1100]$. The outcomes of the simulation show that,

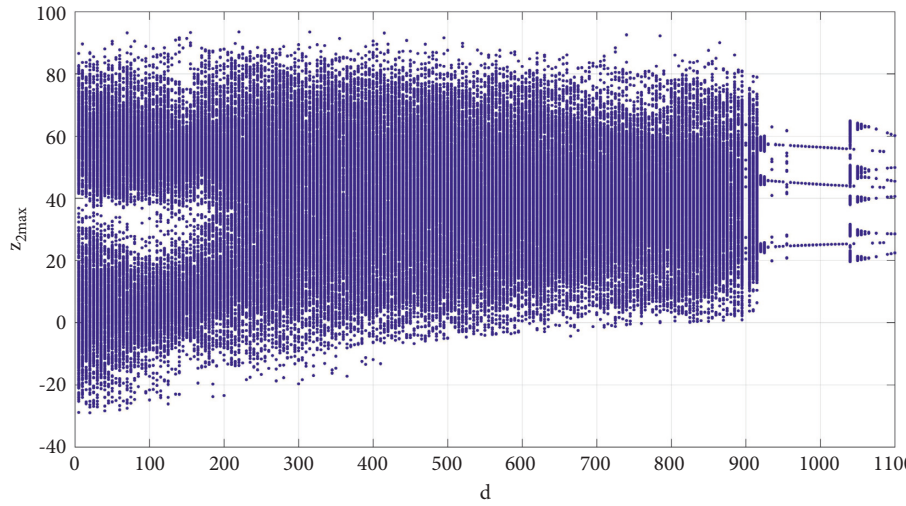

FIGURE 20: Bifurcation diagram for the model (1) when d varies in $[0, 1100]$ and $(a, b, c) = (25, 8, 90)$.

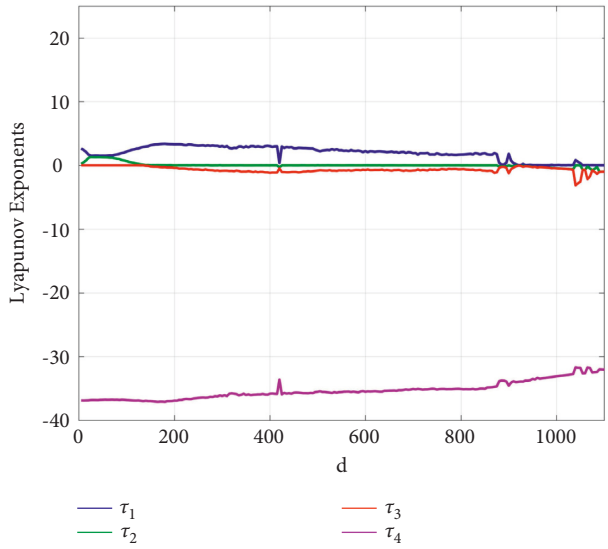

FIGURE 21: Lyapunov exponents for the model (1) when d varies in $[0, 1100]$ and $(a, b, c) = (25, 8, 90)$.

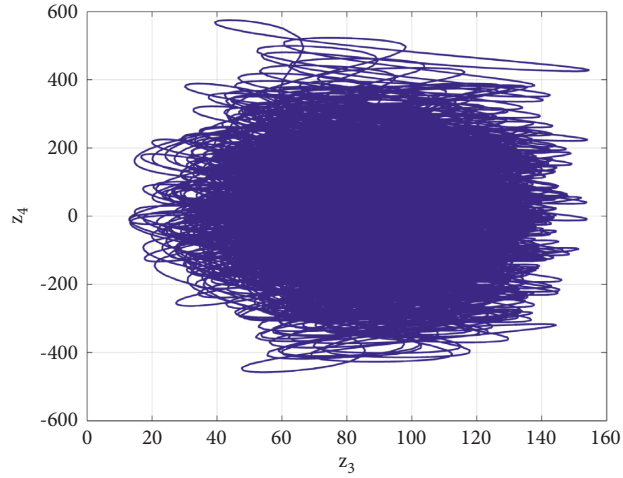

FIGURE 22: A hyperchaotic attractor of the model (1) for $d = 40$ and $(a, b, c) = (25, 8, 90)$.

depending on the value of parameter d, system (1) can display a variety of types of behavior such as periodic, chaotic, or hyperchaotic behavior with varying degrees of complexity. Figure 20 displays the bifurcation diagram for system (1). Figure 21 depicts the LE spectrum $(\tau_1, \tau_2, \tau_3, \tau_4)$ for system (1).

When $5 < d < 140$, system (1) possesses two positive LE values. Figure 22 shows the hyperchaotic attractor of system (1) when $d = 40$. The corresponding LE values of (1) are estimated using MATLAB as follows:

$$\tau_1 = 1.525, \tau_2 = 1.296, \tau_3 = 0, \tau_4 = -36.825. \quad (27)$$

Also, the Kaplan–Yorke dimension of (1) for $d = 40$ is obtained as:

$$D_{KY} = 3 + \frac{\tau_1 + \tau_2 + \tau_3}{|\tau_4|} = 3.0766. \quad (28)$$

We define $C = [140, 875] \cup [1035, 1065]$. When $d \in C, \tau_2$ decreases from a positive value to zero while τ_1 stays still positive. This transition indicates that system (1) has a chaotic response for this very wide region. When $d = 180, \tau_1$ reaches its largest value of 3.392.

Figure 23 shows the chaotic attractor of system (1). The corresponding LE values of (1) are estimated using MATLAB as follows:

$$\tau_1 = 3.392, \tau_2 = 0, \tau_3 = -0.316, \tau_4 = -37.089. \quad (29)$$

Also, the Kaplan–Yorke dimension of (1) for $d = 180$ is obtained as

$$D_{KY} = 3 + \frac{\tau_1 + \tau_2 + \tau_3}{|\tau_4|} = 3.0829. \quad (30)$$

When $d = 1045$, τ_1 decreases to 0.544 providing less strength to the system's chaotic dynamics. Figure 24 shows

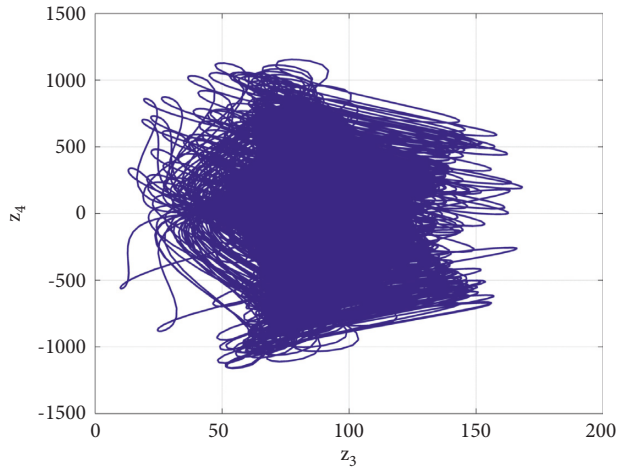

Figure 23: A chaotic attractor of the model (1) for $d = 180$ and $(a, b, c) = (25, 8, 90)$.

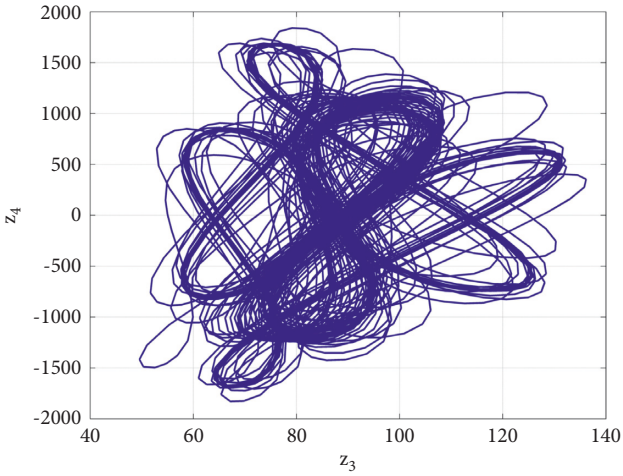

Figure 24: A chaotic attractor of the model (1) for $d = 1045$ and $(a, b, c) = (25, 8, 90)$.

the chaotic attractor of system (1). The corresponding LE values of (1) are estimated using MATLAB as follows:

$$\tau_1 = 0.544, \tau_2 = 0, \tau_3 = -2.811, \tau_4 = -31.735. \quad (31)$$

Also, the Kaplan–Yorke dimension of (1) for $d = 1045$ is obtained as

$$D_{KY} = 2 + \frac{\tau_1 + \tau_2}{|\tau_3|} = 2.1935. \quad (32)$$

We define $D = [875, 1035] \cup [1065, 1100]$. When $d \in D$, there are no positive LE values which means that system (1) has a periodic response in this region of constants. The periodic orbit is shown in Figure 25 when $d = 1020$.

The corresponding LE values of (1) are estimated using MATLAB as follows:

$$\tau_1 = 0, \tau_2 = -0.550, \tau_3 = -0.555, \tau_4 = -32.901. \quad (33)$$

Figures 22–25 portray a 2-D plot of the attractor of the 4-D system (1) in (z_3, z_4) coordinate plane for different values of the constant d while $(a, b, c) = (25, 8, 90)$.

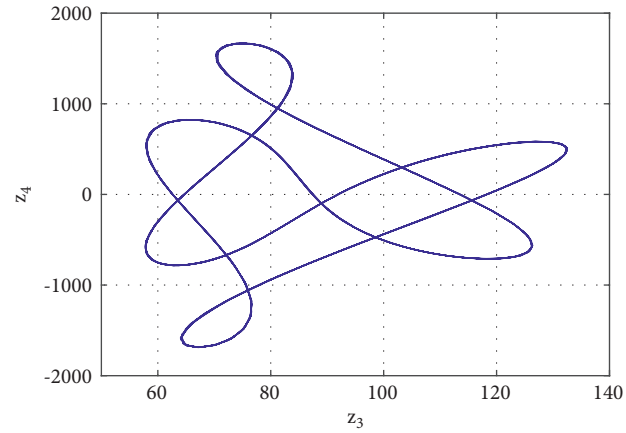

Figure 25: A periodic attractor of the model (1) for $d = 1020$ and $(a, b, c) = (25, 8, 90)$.

4. Coexisting Attractors and Multistability for the New System

Multistability, often referred to as coexisting attractors, is a special nonlinear phenomenon wherein two or more distinct attractors evolve simultaneously from various starting points.

Let Z_{01} and Z_{02} represent two distinct starting points for the new 4-D system (1), where:

$Z_0 = (0.5, 0.5, 0.5, 0.5)$ (Blue color).

$W_0 = (-0.5, -0.5, 0.5, -0.5)$ (Red color).

First, we fix the system constants as $a = 25$, $b = 8$, $c = 32$, and $d = 6$. As shown in Figure 26, system (1) exhibits two different coexisting attractors. The blue one is a periodic attractor that begins from Z_0 and characterized by the following LE spectrum:

$$\tau_1 = 0, \tau_2 = -0.312, \tau_3 = -0.741, \tau_4 = -32.950. \quad (34)$$

The red one is a chaotic attractor that begins from W_0 and characterized by the following LE spectrum:

$$\tau_1 = 0.041, \tau_2 = 0, \tau_3 = -1.111, \tau_4 = -32.928. \quad (35)$$

Next, we fix the system constants as $a = 25$, $b = 14$, $c = 90$, and $d = 6$ As shown in Figure 27, system (1) exhibits two different coexisting chaotic attractors. The blue chaotic attractor begins from Z_0 and characterized by the following LE spectrum:

$$\tau_1 = 0.322, \tau_2 = 0, \tau_3 = -0.393, \tau_4 = -39.942. \quad (36)$$

The red chaotic attractor begins from W_0 and characterized by the following LE spectrum:

$$\tau_1 = 0.236, \tau_2 = 0, \tau_3 = -0.396, \tau_4 = -39.842. \quad (37)$$

Finally, we fix the system constants as $a = 25$, $b = 8$, $c = 65$, and $d = 6$. As shown in Figure 28, system (1) exhibits two different coexisting hyperchaotic attractors. The blue hyperchaotic attractor begins from Z_0 and characterized by the following LE spectrum:

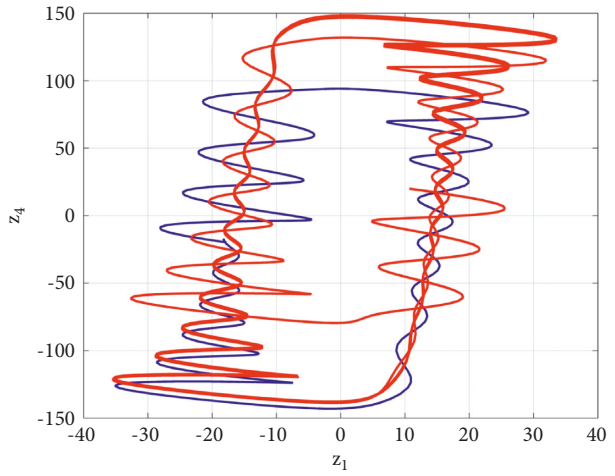

Figure 26: The coexistence of one periodic and one chaotic attractor for system (1) projected in the (z_1, z_4) coordinate plane for the choice of parameters $(a, b, c, d) = (25, 8, 32, 6)$.

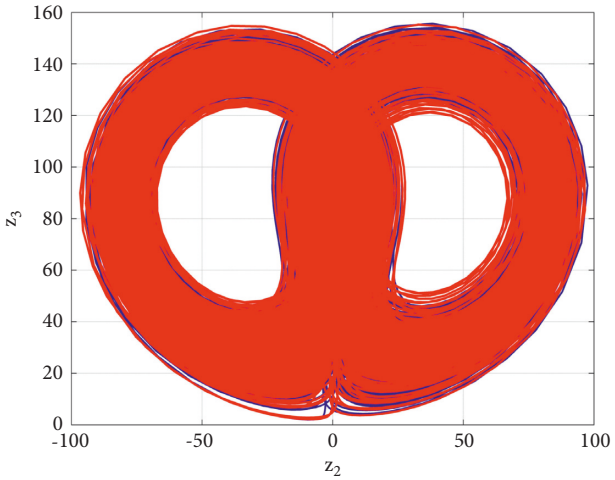

Figure 27: The coexistence of chaotic attractors for system (1) projected in the (z_2, z_3) coordinate plane for the choice of parameters $(a, b, c, d) = (25, 14, 90, 6)$.

$$\tau_1 = 1.970, \tau_2 = 0.341, \tau_3 = 0, \tau_4 = -36.313. \quad (38)$$

The red hyperchaotic attractor begins from W_0 and characterized by the following LE spectrum:

$$\tau_1 = 1.958, \tau_2 = 0.339, \tau_3 = 0, \tau_4 = -36.300. \quad (39)$$

5. Electronic Circuit Design for the New Hyperchaotic Two-Scroll System

We detail the electronic circuit realization of the proposed two-scroll hyperchaotic model using MultiSim software (Version 14). Figure 29 depicts an analog electronic circuit for the implementation of the proposed hyperchaotic circuit, which includes two analog multipliers (AD63JN), seven

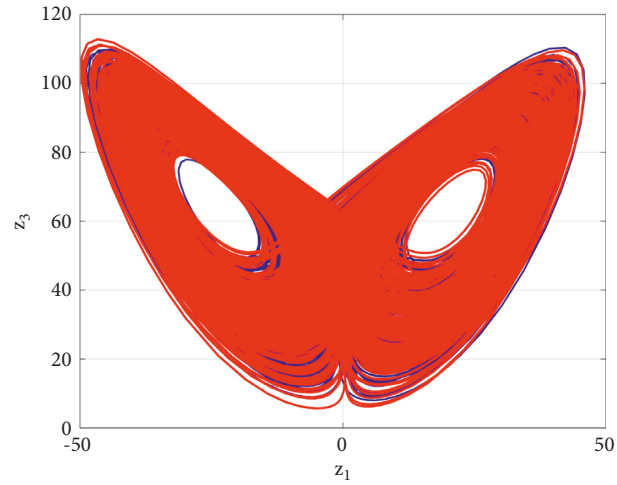

Figure 28: The coexistence of hyperchaotic attractors for system (1) projected in the (z_1, z_3) coordinate plane for the choice of parameters $(a, b, c, d) = (25, 8, 65, 6)$.

operational amplifiers (TL083CD), seventeen resistors, and four capacitors.

For the circuit design, we rescale the two-scroll model (1) using the following transformation of coordinates:

$$Z_i = \frac{1}{2} z_i, \ (i = 1, 2, 3, 4). \quad (40)$$

Replacing the old variables with the new variables on the new 4-D hyperchaotic system (1), we obtain the following system:

$$\begin{cases} \dot{Z}_1 = a(Z_2 - Z_1) - Z_3 + Z_4, \\ \dot{Z}_2 = cZ_1 - Z_2 - 2Z_1Z_3 + Z_4, \\ \dot{Z}_3 = -bZ_3 + 2Z_1Z_2, \\ \dot{Z}_4 = -dZ_2. \end{cases} \quad (41)$$

Using Kirchhoff's electrical circuit laws, we derive the circuit model for the rescaled hyperchaotic model (41) as follows:

$$\begin{cases} C_1\dot{Z}_1 = \frac{1}{R_1}Z_2 - \frac{1}{R_2}Z_1 - \frac{1}{R_3}Z_3 + \frac{1}{R_4}Z_4, \\ C_2\dot{Z}_2 = \frac{1}{R_5}Z_1 - \frac{1}{R_6}Z_2 - \frac{1}{10R_7}Z_1Z_3 + \frac{1}{R_8}Z_4, \\ C_3\dot{Z}_3 = -\frac{1}{R_9}Z_3 + \frac{1}{10R_{10}}Z_1Z_2, \\ C_4\dot{Z}_4 = -\frac{1}{R_{11}}Z_2. \end{cases} \quad (42)$$

Here, Z_1, Z_2, Z_3, Z_4 are the voltages across the capacitors, C_1, C_2, C_3, C_4, respectively. We choose the values of the circuital elements as follows:

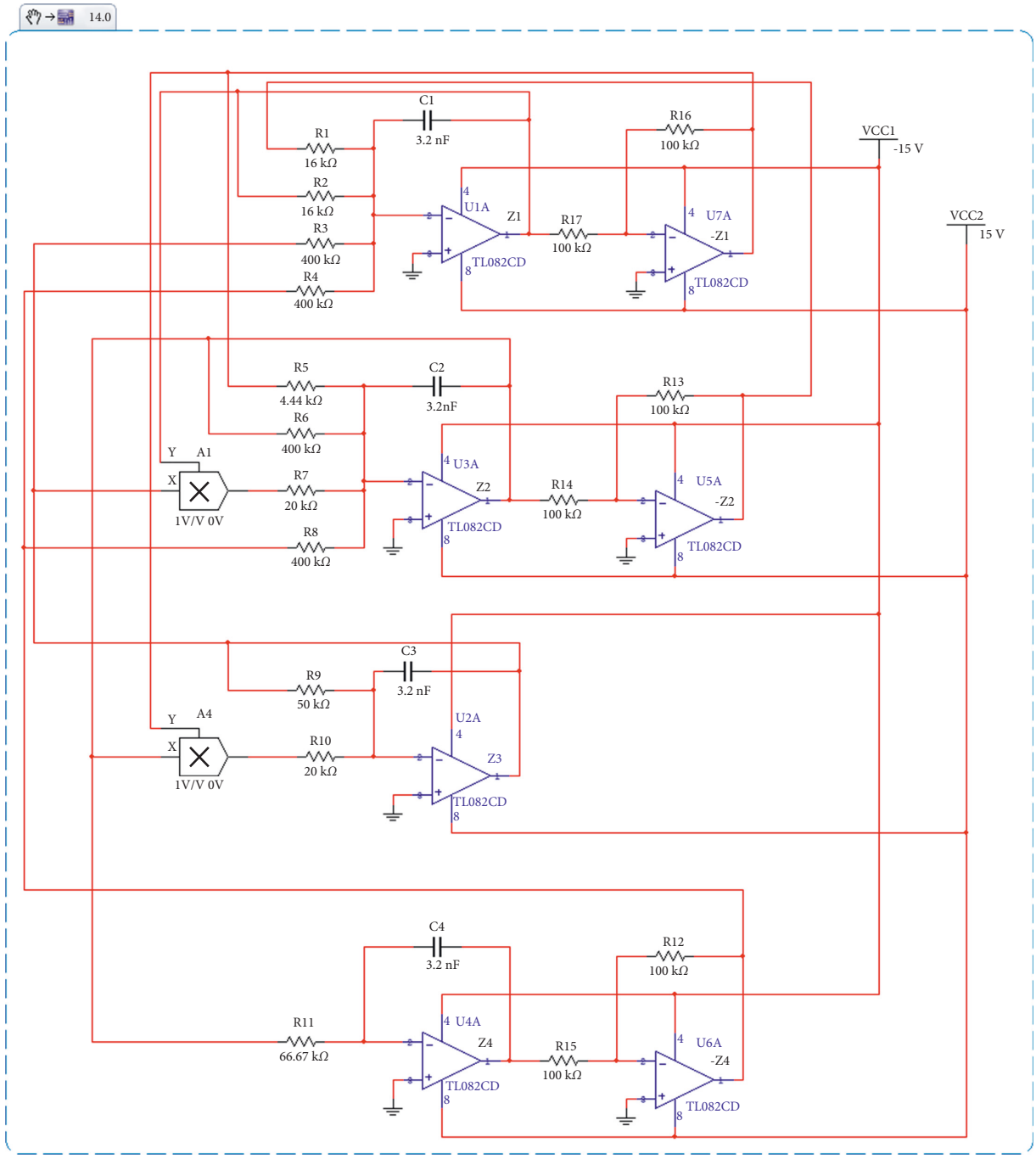

Figure 29: The electronic circuit design for the 4-D hyperchaotic system (29).

$R_1 = R_2 = 16k\Omega$, $R_3 = R_4 = R_6 = R_8 = 400k\Omega$, $R_5 = 4.44k\Omega$,

$R_7 = R_{10} = 20k\Omega$, $R_9 = 50k\Omega$, $R_{11} = 66.67k\Omega$,

$R_{12} = R_{13} = R_{14} = R_{15} = R_{16} = R_{17} = 100k\Omega$,

$C_1 = C_2 = C_3 = C_4 = 3.2nF$.

With MultiSim 14.0, we obtain the experiment observations of system (42) in Figures 30–33. It can be seen that the good qualitative agreement between the MATLAB simulations (Figures 1–4) and the MultiSim results (Figures 30–33) of the hyperchaotic two-scroll system is confirmed.

6. FPGA Implementation of the New Two-Scroll Hyperchaotic Model

The use of field-programmable gate arrays (FPGA) has shown advantages in the implementation of chaotic and hyperchaotic systems, as done in [31–34]. One can find guidelines on applying numerical methods that are directly

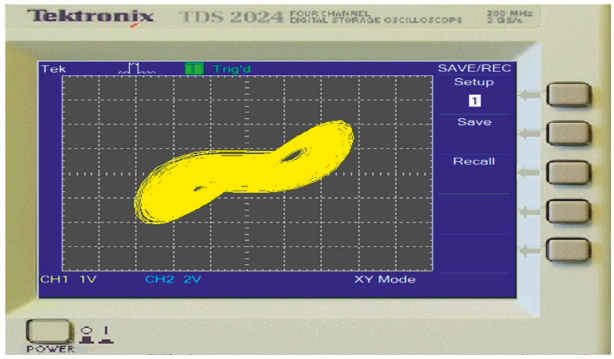

Figure 30: Electronic circuit simulation using MultiSim 14.0 for the new hyperchaotic two-scroll circuit (42) in the (Z_1, Z_2)– coordinate plane.

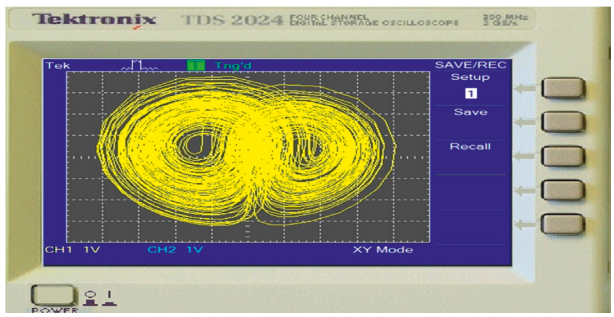

Figure 31: Electronic circuit simulation using MultiSim 14.0 for the new hyperchaotic two-scroll circuit (42) in the (Z_2, Z_3)– coordinate plane.

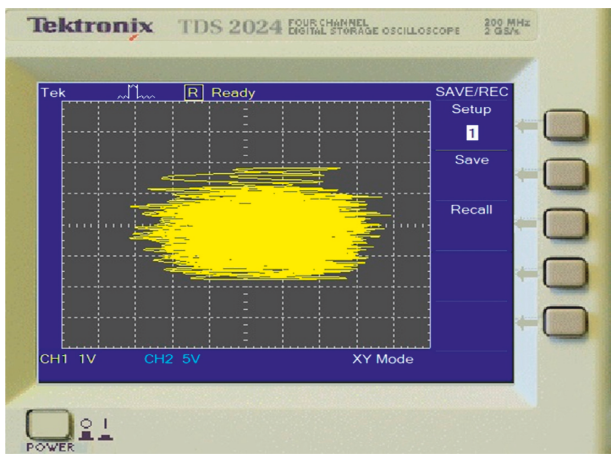

Figure 32: Electronic circuit simulation using MultiSim 14.0 for the new hyperchaotic two-scroll circuit (42) in the (Z_3, Z_4)– coordinate plane.

synthesized into an FPGA [35]. In this work, we show the experimental results of the FPGA implementation of proposed model (1) by applying two common numerical methods. The first one is the forward Euler, whose iterative algorithm is given in equation (30), and the second one is the

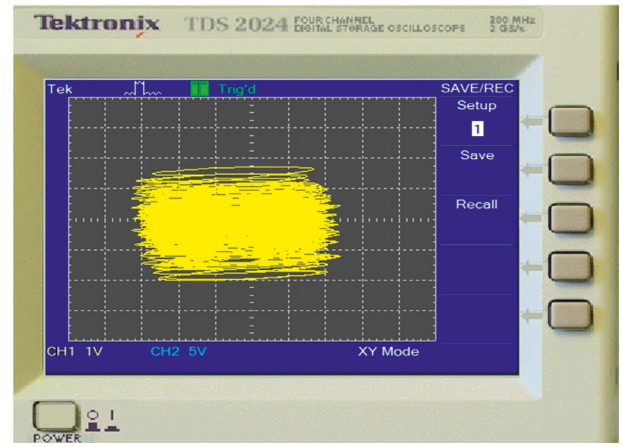

Figure 33: Electronic circuit simulation using MultiSim 14.0 for the new hyperchaotic two-scroll circuit (42) in the (Z_1, Z_4)– coordinate plane.

implicit algorithm known as trapezoidal method that is given in equation (31).

$$x_{n+1} = x_n + hf(x_n, t_n),$$
$$x_{n+1} = x_n + \frac{h}{2}[f(x_n, t_n) + f(x_{n+1}, t_{n+1})]. \quad (43)$$

It is well-known that a system of ordinary differential equations, as the one associated for the proposed model (1), can be solved by discretizing the equations using a numerical method. In the case of applying the forward Euler, one gets the discrete equations given by equation (44), from which one can clearly see the requirement of arithmetic operations as adders, subtractors, and multipliers. The control of the iterations is performed by designing a state machine control that includes registers, as detailed in [35], where one can see the design of the arithmetic blocks, and a single-constant multiplier block to reduce hardware resources.

$$\begin{cases} z_1[n+1] = z_1[n] + h(a(z_2[n] - z_1[n]) - z_3[n] + z_4[n]), \\ z_2[n+1] = z_2[n] + h(cz_1[n] - z_2[n] - z_1[n]z_3[n] + z_4[n]), \\ z_3[n+1] = z_3[n] + h(-bz_3[n] + z_1[n]z_2[n]), \\ z_4[n+1] = z_4[n] + h(-dz_2[n]). \end{cases} \quad (44)$$

The design of each digital block requires the definition of the number of bits to be processed. In this case, the computer arithmetic is performed by applying fixed-point representation with the format 15.49. The 64 bits are distributed in one bit for the sign, 14 for the integer part, and 49 bit for the fractional part. The bit distribution considers the maximum amplitude values that can appear for each state variable during the processing of the data. For example, from the simulation results of the new 4-D hyperchaotic system (1), the four state variables have amplitudes in the range $[-199.02, 342.50]$, but in the discretization process by applying the numerical methods, an analysis of all the internal arithmetic operations, mainly those that result during the

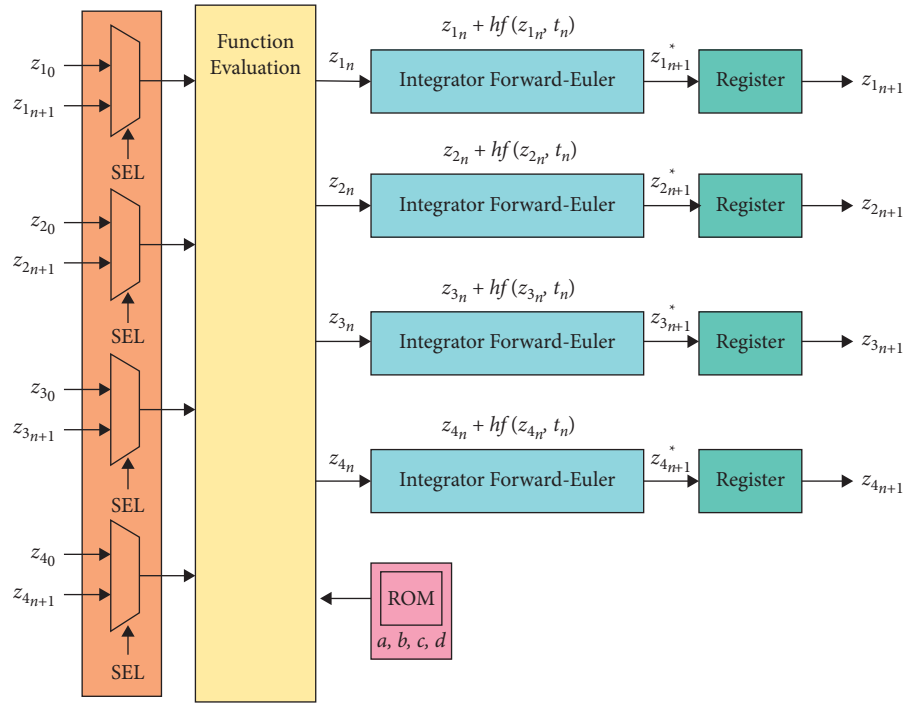

Figure 34: Block diagram of the discretization of the proposed model (1) using the forward Euler method.

Table 1: Hardware resources for the FPGA design of (1) using the FPGA basys 3 xilinx artix-7 XC7A35T-ICPG236C using two numerical methods with $h = 0.001$.

Resources	Forward Euler	Trapezoidal	Available
LUTs	4679	10570	20,800
FF	567	1253	41,600
DSP	45	82	90
Multipliers	10	24	–
Adders	5	18	–
Subtractors	6	12	–
Clock cycles by iteration	2	3	–
Latency (ns)	80	120	–

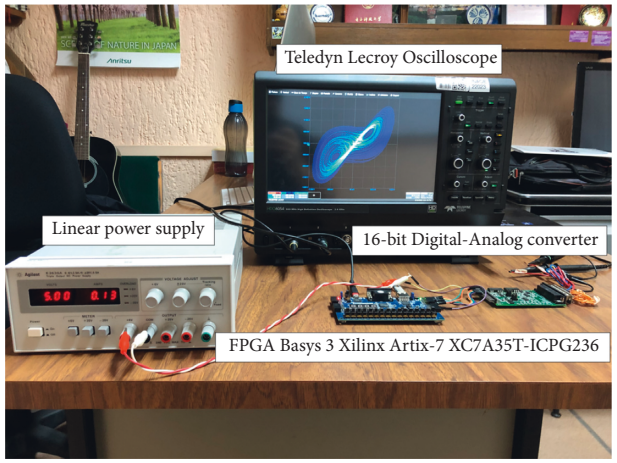

Figure 35: Experimental setup to measure the attractors of the proposed model (1) using a FPGA basys 3 xilinx artix-7 XC7A35T-ICPG236, a 16 bit digital-analog converter, a linear power supply and a keysight oscilloscope to visualize the hyperchaotic attractor.

multiplications among state variables, resulted in an absolute range of values in the range $[-11299.60, 11116.51]$, thus leading to use the format 15.49.

Figure 34 depicts a block diagram showing the discretization of the proposed model (1) using the forward Euler method given in equation (32). The registers are controlled by a state machine to perform the iteration process. The FPGA implementation is also done in a similar way by applying the trapezoidal method so that the hardware resources for the FPGA design using the FPGA Basys 3 Xilinx Artix-7 XC7A35T-ICPG236C are as summarized in Table 1. One can see the number of lookup tables (LUTs), flip-flops (FF), digital signal processors (DSP), multipliers, adders, and subtractors. We also give the number of clock cycles required by an iteration, and the latency in nanoseconds (ns).

The FPGA experimental setup for the proposed model (1) is shown in Figure 35. Furthermore, the FPGA experimental outputs of (1) are depicted in Figures 36–39.

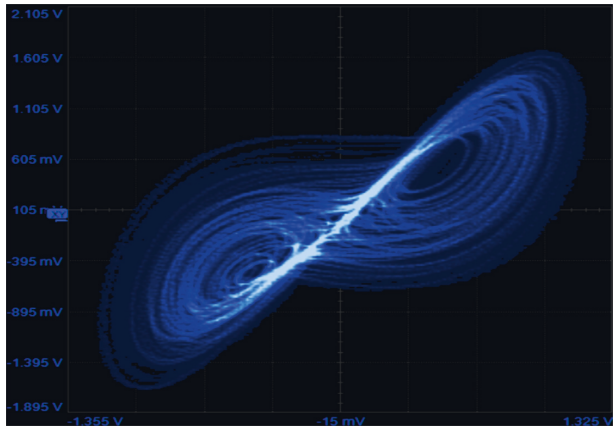

Figure 36: Experimental hyperchaotic attractor of the proposed model (1) in the $(z_1, z_2)-$ plane.

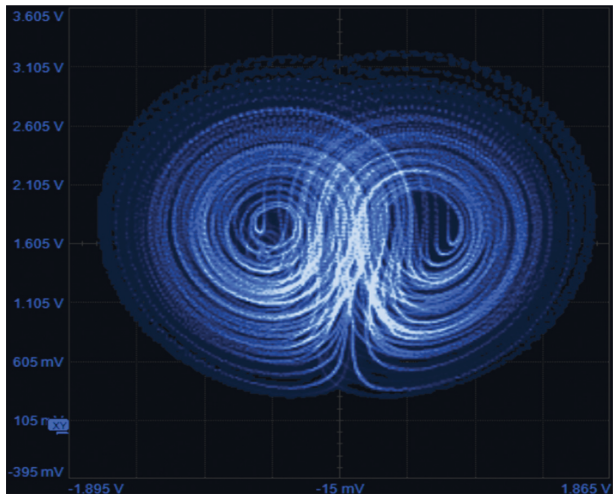

Figure 37: Experimental hyperchaotic attractor of the proposed model (1) in the $(z_2, z_3)-$ plane.

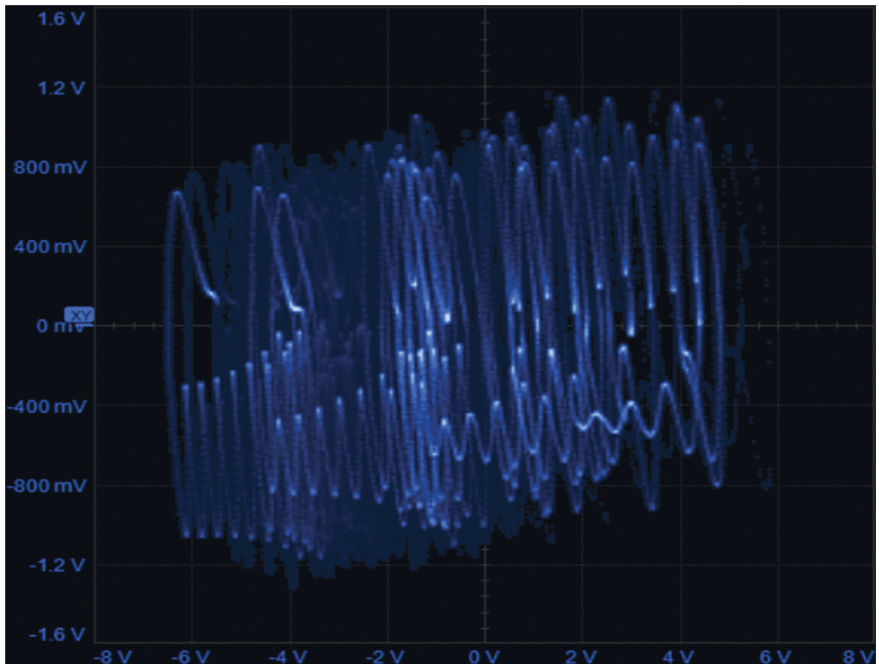

Figure 38: Experimental hyperchaotic attractor of the proposed model (1) in the $(z_3, z_4)-$ plane.

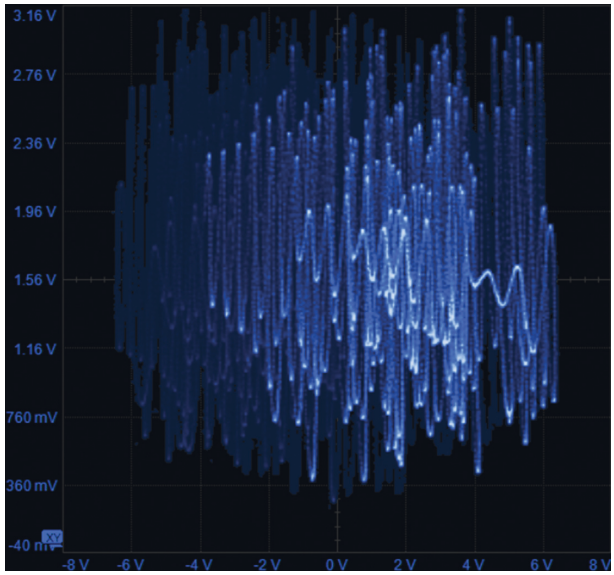

Figure 39: Experimental hyperchaotic attractor of the proposed model (1) in the $(z_1, z_4)-$ plane.

7. Conclusions

In this research work, we reported our findings of a new four-dimensional two-scroll hyperchaotic system having only two quadratic nonlinearities. We conducted a detailed dynamic study of the proposed model and noted the coexistence of attractors for fixed parameter values but different initial states. Since the maximal Lyapunov exponent (MLE) of the two-scroll system is $\tau_{\max} = 2.6174$, we deduced that the two-scroll system (1) has high complexity. Also, a design for an electronic circuit has been made for the new hyperchaotic system using MultiSim (Version 14). The experimental observation of the hyperchaotic attractors has been shown from the FPGA implementation by applying numerical methods, *viz*. forward Euler method and trapezoidal method. It was observed that the FPGA experimental results using the forward Euler discretization method are in good agreement with the MATLAB simulation results of the proposed hyperchaotic two-scroll system.

Data Availability

The data used for this research paper are available on request from the corresponding author.

Conflicts of Interest

The authors declare no conflicts of interest on the publication of this paper.

References

[1] Y. Wang, H. Li, G. Yan, and M. Chen, "Predefined-time chaos synchronization of memristor chaotic systems by using simplified control inputs," *Chaos, Solitons & Fractals*, vol. 161, Article ID 112282, 2022.

[2] Y. Dong, S. Yang, Y. Liang, and G. Wang, "Neuromorphic dynamics near the edge of chaos in memristive neurons," *Chaos, Solitons & Fractals*, vol. 160, Article ID 112241, 2022.

[3] H. L. Luo, D. W. Ding, Z. L. Yang, and H. Xiao, "Coexisting behaviors of chaotic system with tri-stable locally active memristor and its application in color image encryption," *The European Physical Journal Plus*, vol. 137, no. 5, Article ID 607, 2022.

[4] X. Wu, S. He, W. Tan, and H. Wang, "From memristor-modeled jerk system to the nonlinear systems with memristor," *Symmetry*, vol. 14, no. 4, Article ID 659, 2022.

[5] Y. J. F. Kpomahou, A. Adomou, A. E. Yamadjako, and J. Djossou, "Effect of amplitude-modulated force on horseshoe dynamics in Briggs–Rauscher chemical system modeled by a new parametric oscillator with asymmetric potential," *The European Physical Journal Plus*, vol. 137, no. 6, Article ID 679, 2022.

[6] A. J. Adéchinan, Y. J. F. Kpomahou, L. A. Hinvi, and C. H. Miwadinou, "Chaos, coexisting attractors and chaos control in a nonlinear dissipative chemical oscillator," *Chinese Journal of Physics*, vol. 77, pp. 2684–2697, 2022.

[7] S. Liu, Z. Sun, N. Zhao, and W. Xu, "Explosive transition in coupled oscillators through mixed attractive-repulsive interaction," *International Journal of Bifurcation and Chaos*, vol. 32, no. 2, Article ID 2250018, 2022.

[8] H. Zhang, Z. Qin, Y. Zhang, D. Chen, J. Gen, and H. Qin, "A practical underwater information sensing system based on intermittent chaos under the background of Lévy noise," *EURASIP Journal on Wireless Communications and Networking*, vol. 2022, no. 1, Article ID 41, 2022.

[9] W. Bao and C. Zhu, "A secure and robust image encryption algorithm based on compressive sensing and DNA coding," *Multimedia Tools and Applications*, vol. 81, no. 11, pp. 15977–15996, 2022.

[10] H. Zhou, H. Xie, H. Zhang, and H. Zhang, "Parallel remote sensing image encryption algorithm based on chaotic map and DNA encoding," *Journal of Image and Graphics*, vol. 26, no. 5, pp. 1081–1094, 2022.

[11] X. Gong, H. Wang, Y. Ji, and Y. Zhang, "Optical chaos generation and synchronization in secure communication with electro-optic coupling mutual injection," *Optics Communications*, vol. 521, Article ID 128565, 2022.

[12] S. Xiang, M. Yang, and J. Wang, "Chaotic optical communications of 12.5-Gbaud OOK and 10-Gbaud QPSK signals based on mutual injection of semiconductor lasers," *Optics Letters*, vol. 47, no. 11, pp. 2818–2821, 2022.

[13] N. Biswas and R. Mohamed I, "DCSK performance analysis of a chaos-based communication using a newly designed chaotic system," *International Journal of Nonlinear Sciences and Numerical Stimulation*, vol. 23, no. 3-4, pp. 579–592, 2022.

[14] G. Arthi, V. Thanikaiselvan, and R. Amirtharajan, "4D Hyperchaotic map and DNA encoding combined image encryption for secure communication," *Multimedia Tools and Applications*, vol. 81, no. 11, pp. 15859–15878, 2022.

[15] B. S. Yu, Y. N. Tang, and K. Ji, "Chaotic behaviors of an in-plane tethered satellite system with elasticity," *Acta Astronautica*, vol. 193, pp. 395–405, 2022.

[16] W. Quan, H. Wang, and Y. Ji, "Three-loop electro-optical phase chaotic secure communication system with time-delay signatures concealment and key space enhancement," *Optics Communications*, vol. 512, Article ID 128065, 2022.

[17] C. Xiu, J. Fang, and Y. Liu, "Design and circuit implementation of a novel 5D memristive CNN hyperchaotic

system," *Chaos, Solitons & Fractals*, vol. 158, Article ID 112040, 2022.

[18] H. Nazir, I. S. Bajwa, S. Abdullah, R. Kazmi, and M. Samiullah, "A color image encryption scheme combining hyperchaos and genetic codes," *IEEE Access*, vol. 10, pp. 14480–14495, 2022.

[19] Y. Y. Bian and W. X. Yu, "A secure communication method based on 6-D hyperchaos and circuit implementation," *Telecommunication Systems*, vol. 77, no. 4, pp. 731–751, 2021.

[20] M. Boumaraf and F. Merazka, "Secure speech coding communication using hyperchaotic key generators for AMR-WB codec," *Multimedia Systems*, vol. 27, no. 2, pp. 247–269, 2021.

[21] A. Ibraheem, "Switched dual compound–compound anti-synchronization of hyperchaotic dynamical systems," *International Journal of Algorithms, Computing and Mathematics*, vol. 8, no. 3, Article ID 122, 2022.

[22] M. Tang, G. Zeng, Y. Yang, and J. Chen, "A hyperchaotic image encryption scheme based on the triple dislocation of the Liu and Lorenz system," *Optik*, vol. 261, Article ID 169133, 2022.

[23] S. Li, Y. Wu, and G. Zheng, "Adaptive synchronization for hyperchaotic liu system," *Frontiers in Physics*, vol. 9, Article ID 812048, 2022.

[24] Y. Xiao, S. Zhang, and Y. Peng, "Dynamic investigations in a Stackelberg model with differentiated products and bounded rationality," *Journal of Computational and Applied Mathematics*, vol. 414, Article ID 114409, 2022.

[25] T. Peixe and A. Rodrigues, "Persistent strange attractors in 3D polymatrix replicators," *Physica D: Nonlinear Phenomena*, vol. 438, Article ID 133346, 2022.

[26] B. Zhou, Y. Jin, and H. Xu, "Subharmonic resonance and chaos for a class of vibration isolation system with two pairs of oblique springs," *Applied Mathematical Modelling*, vol. 108, pp. 427–444, 2022.

[27] S. Vaidyanathan, K. Benkouider, and A. Sambas, "A new multistable jerk chaotic system, its bifurcation analysis, backstepping control-based synchronization design and circuit simulation," *Archives of Control Sciences*, vol. 32, no. 1, pp. 123–152, 2022.

[28] S. S. De Sarkar, A. K. Sharma, and S. Chakraborty, "Chaos, antimonotonicity and coexisting attractors in Van der Pol oscillator based electronic circuit," *Analog Integrated Circuits and Signal Processing*, vol. 110, no. 2, pp. 211–229, 2022.

[29] P. Boriskov, "Chaotic LIF oscillator with variable resistance feedback and nonlinear rate coding," *IEEE Transactions on Circuits and Systems II: Express Briefs*, vol. 69, no. 6, pp. 2982–2986, 2022.

[30] S. Yan, Z. Song, and W. Shi, "Symmetric coexisting attractors in a novel memristors-based Chuas chaotic system," *Journal of Circuits, Systems, and Computers*, vol. 31, no. 07, Article ID 2250120, 2022.

[31] M. D. Gupta and R. K. Chauhan, "Hardware efficient pseudo-random number generator using chen chaotic system on FPGA," *Journal of Circuits, Systems, and Computers*, vol. 31, no. 03, Article ID 2250043, 2022.

[32] W. A. Al-Musawi, W. A. Wali, and M. A. Ali Al-Ibadi, "Field-programmable gate array design of image encryption and decryption using Chua's chaotic masking," *International Journal of Electrical and Computer Engineering*, vol. 12, no. 3, pp. 2414–2424, 2022.

[33] S. Cang, L. Wang, Y. Zhang, Z. Wang, and Z. Chen, "Bifurcation and chaos in a smooth 3D dynamical system extended from Nose-Hoover oscillator," *Chaos Solitons*, vol. 158, no. 2, Article ID 112016, 2022.

[34] H. Jia, Z. Chen, W. Shi, and G. Qi, "A new generalized Hamiltonian chaotic system with transient quasi-periodic flows and intermittent chaos," *International Journal of Bifurcation and Chaos*, vol. 32, no. 2, 2022.

[35] M. Alcin, M. Tuna, P. Erdogmus, and I. Koyuncu, "FPGA-based dual core TRNG design using Ring and Runge-Kutta-Butcher based on chaotic oscillator," *Chaos Theory and Applications*, vol. 3, no. 1, pp. 20–28, 2021.